Structure of VAT, a CDC48/p97 ATPase homologue from the archaeon *Thermoplasma acidophilum* as studied by electron tomography

Beate Rockel, Jochen Walz, Reiner Hegerl, Jürgen Peters, Dieter Typke, Wolfgang Baumeister*

Max-Planck-Institut für Biochemie, Abteilung für molekulare Strukturbiologie, Am Klopferspitz 18a, D-82152 Martinsried, Germany

Received 16 March 1999

Abstract Valosine-containing protein-like ATPase from *Thermoplasma acidophilum* is a member of the superfamily of ATPases associated with a diversity of cellular activities and is closely related to CDC48 from yeast and p97 from higher eukaryotes and more distantly to *N*-ethylmaleimide-sensitive fusion protein. We have used electron tomography to obtain low-resolution (2–2.5 nm) three-dimensional maps of both the whole 500 kDa complex and the N-terminally truncated valosine-containing protein-like ATPase from *T. acidophilum* complex lacking the putative substrate binding domain.

Key words: ATPases associated with a diversity of cellular activities; Valosine-containing protein-like ATPase from *Thermoplasma acidophilum*; Electron tomography; *Thermoplasma acidophilum*

1. Introduction

The AAA-protein family (for ATPases associated with a diversity of cellular activities [1]) belongs to the large family of Walker-type ATPases which is defined by the consensus motifs Walker A and B [2]. The presence of an additional region of high sequence conservation, termed the second region of homology (SRH), distinguishes AAA-ATPases from other Walker-type ATPases. A sequence stretch of 200–250 amino acid residues which encompasses the Walker A and B motifs and the SRH is referred to as the AAA-module and can be present in either one or two copies in AAA-proteins. Members of the AAA-family are found in all three domains of life and fulfil a large variety of tasks in different cellular processes. Based on sequence comparisons, AAA-proteins have been further divided into a number of distinct subfamilies [3,4].

Members of subfamily 1 contain two fully conserved AAA-modules [5]. A N-terminal domain comprising 180–240 amino acid residues precedes these AAA-modules. CDC48 of *Saccharomyces cerevisiae* [6] and p97 of vertebrates, also known as valosine-containing protein (VCP) [7], are well-characterized members of this subfamily. VCP-like ATPase from *Thermoplasma acidophilum* (VAT) was recently shown to belong to this subfamily [8] and other archaeal homologues have been identified in several sequenced genomes. Eukaryotic members of subfamily 1, such as p97 and CDC48, are involved in homotypic membrane fusion events [9,10]. The cellular functions of their archaeal homologues are still enigmatic.

One of the best studied AAA-proteins is *N*-ethylmaleimide-sensitive fusion protein (NSF). It belongs to subfamily 4 of the AAA-proteins [5] and it is required for vesicular transport between the endoplasmic reticulum and the Golgi stack [11,12] as well as for the fusion of synaptic vesicles with the presynaptic membrane during neurotransmission [13]. More specifically, NSF is believed to dissociate the membrane fusion machinery after one round of fusion and to prepare it for the next round. Each 85 kDa subunit of NSF consists of three domains: N (the N-terminal domain), D1 (which contains the first AAA-module) and D2 (that includes the second AAA-module) [14,15]. In NSF, the N domain is the putative substrate binding domain, while D1 is essential for the membrane fusion activity and D2 appears to promote oligomerization [16,17]. NSF and members of the subfamily 1 share the same domain organization, N-D1-D2 (Fig. 1a). However, the role of these three domains has not yet been defined for members of subfamily 1.

Electron microscopy (EM) has shown that p97 from *Xenopus laevis* [18], VAT from *T. acidophilum* [8], CDC48 from *S. cerevisiae* [19], as well as NSF from *Cricetulus griseus* [20] form hexameric ring complexes. Quick-freeze deep-etch EM of NSF has shown that the protein is a hollow cylinder (10×16 nm) that undergoes large-scale conformational changes upon nucleotide binding. The N domain of NSF which appears to be rather flexible linked to the core complex is believed to be the substrate binding domain [21]. Recently, the crystal structures of both the AAA-modules of the clamp loader complex of *Escherichia coli* DNA polymerase III [22] and the D2 domain of NSF [23,24] have been determined. The two structures turned out to be remarkably similar. The NSF D2 protomer consists of a small α-helical domain and a wedge-shaped nucleotide binding domain with a central five-stranded parallel β-sheet flanked by α-helices. In the NSF D2 hexamer, these flanking helices provide the contacts between adjacent protomers. The hexamer, that has a diameter of approximately 12 nm and a height of approximately 4 nm encloses a central channel of about 1.8 nm width.

In order to have a better understanding of the mechanism of action of subfamily 1 and 4 AAA-proteins, a detailed picture of the entire complex is required. To this end, we performed electron tomography studies on the VAT complex

*Corresponding author. Fax: (49) (89) 8578 2641.
E-mail: baumeist@biochem.mpg.de

Abbreviations: CDC48, cell division cycle protein 48; HEPES, 2-(4-(2-hydroxyethyl)-1-piperazinyl)-ethanesulfonic acid; MES, 2-(*N*-morpholino)ethanesulfonic acid; NSF, *N*-ethylmaleimide-sensitive fusion protein; PAGE, polyacrylamide gel electrophoresis; PMSF, phenylmethylsulfonyl fluoride; SDS, sodium dodecyl sulfate

0014-5793/99/$20.00
PII: S0014-5793(99)00431-7

from *Thermoplasma* and on an N-terminally truncated mutant.

2. Materials and methods

2.1. Protein expression and purification

The expression and isolation of recombinant VAT from *E. coli* cells was performed as described previously [8]. Following size exclusion chromatography on a Superose 6 column, VAT protein was kept in a buffer containing 10 mM HEPES, 300 mM NaCl, 10 mM cysteine hydrochloride, pH 8.0, and used either directly for EM investigations or stored at −80°C.

In order to create a mutant in which the N domain of 183 amino acid residues was deleted, the plasmid carrying the complete gene was cut with *Nde*I and *Stu*I. A synthetic linker was then inserted and, following ligation, the plasmid was cloned into *E. coli* strain BL21(DE3). Protein expressed from this plasmid had a N-terminal methionine residue fused to Val-184 and is denoted as VAT(ΔN) (see Fig. 1). Isolation of recombinant VAT(ΔN) from *E. coli* cells was performed with several modifications of [8]. Bacteria were lysed by sonication in buffer A (20 mM Tris-HCl, pH 7.5, 300 mM NaCl, 1 mM PMSF) before clearing the lysate by centrifugation at 4°C for 20 min at 55 000×*g*. Next, the supernatant was incubated with 2 ml/100 ml Q-Sepharose for several minutes before packing of the slurry into a poly-prep column (Bio-Rad). The eluate was then directly applied to a Ni-NTA column (Quiagen) and washed with 20 mM MES pH 6.3, 300 mM NaCl, 10 mM imidazole. VAT(ΔN) was eluted in 50 mM steps using a discontinuous gradient ranging from 50 up to 400 mM imidazole. Fractions containing predominantly VAT(ΔN) were pooled and applied to a Superose 6 column using 10 mM HEPES, pH 7.5, 150 mM NaCl, 2 mM cysteine as buffer. Following size exclusion chromatography, the pH of fractions containing VAT(ΔN) was adjusted to 8.0 and the protein solution diluted 1:5 in 10 mM Tris, pH 8.0, before application to a HiTrap Q column (Pharmacia). Protein was eluted by a discontinuous gradient of 50–400 mM NaCl in 10 mM Tris, pH 7.5, in steps of 50 mM NaCl. Fractions containing VAT(ΔN) were pooled and $MgCl_2$ was added to a final concentration of 5 mM. The protein solution was then immediately frozen in liquid nitrogen and stored at −80°C. The purity of recombinant protein was monitored by electrophoresis on SDS acrylamide gels according to Schägger and von Jagow [25]. Proteins were visualized by Coomassie staining as described by Neuhoff et al. [26].

2.2. Sample preparation for EM

Carbon-coated copper grids were rendered hydrophilic in a Plasma Cleaner (Harrick Scientific Corporation, New York, USA). 5 μl protein solution was applied to grids for 60 s and then blotted without complete drying of the sample. Subsequently 5 μl of an aqueous solution of either methylamine tungstate (2%) or uranyl acetate (2%) was applied for negative staining. After 30 s, the staining solution was blotted and the grids were used for EM.

2.3. EM and image processing

Data collection for two-dimensional (2-D) analysis and for electron tomography was performed using a Philips CM 200 FEG equipped with a 1K×1K slow-scan CCD camera (Photometrics) and a VIPS 1000 computer with a 'Supercard' (TVIPS) [27]. All off-line image processing steps were performed on SGI workstations (Silicon Graphics, Mountain View, CA, USA) using the EM software package [28,29].

For 2-D analysis, data sets were recorded using CCD spot scanning at magnifications of 27 500× and at a defocus of −800 nm. 1422 VAT particles and 1138 VAT(ΔN) particles, both negatively stained with uranyl acetate, were extracted interactively. The aligned data sets were subjected to an eigenvector-eigenvalue-based classification procedure [30] to detect significant inter-image variations.

For three-dimensional (3-D) analysis, four tomographic tilt series of VAT particles and five tomographic tilt series of VAT(ΔN) particles, both negatively stained with methylamine tungstate, were recorded at magnifications of 20×000× with tilt angles ranging from −75° to +80° and increments of 5°. The cumulative dose for 31–32 images was 10 000–12 000 e^-/nm^2. This dose is regarded as 'subcritical' for negatively stained specimens. The projections of each tilt series were aligned using cross-correlation techniques and volumes of a size of 1024×1024×128 pixels were reconstructed via filtered backprojection using exact filtering [31,32]. From these volumes, 556 and 429 subvolumes of 64×64×64 pixels containing VAT and VAT(ΔN), respectively, were cut out at manually marked x-y-positions. Projections along the z-axis of reconstructed particles were aligned with respect to translation and rotation. The approximate z-positions in the subvolumes were determined by visual inspection. The in-plane rotation of the reconstructed particles was corrected according to the alignment parameters and initial references of VAT and VAT(ΔN) were obtained by adding up all aligned VAT and VAT(ΔN) particles, respectively. Subsequently, 3-D-alignment of subvolumes was performed, averages were calculated and finally 6-fold symmetrized as described in [33]. The resolution of the averages was determined using Fourier Shell correlation [34], taking into account the 6-fold symmetrization of the averages [35]. The threshold curves (3σ) crossed the Fourier Shell correlation curves at a resolution of $\approx 1/22$ $Å^{-1}$ for both averages. Subsequently, the calculated averages of VAT and VAT(ΔN) were low-pass-filtered with a cut-off frequency of 1/22 $Å^{-1}$.

Isosurface representations of the calculated averages were created with the AVS software (Advanced Visual Systems, Waltham, MA, USA). For comparison with crystal structures of the D2 domain of NSF, the Protein Data Bank file containing the coordinates (Brookhaven Protein Data Bank accession number 1D2N) was converted to EM format using the information about atom-type and their coordinates for the calculation of density distributions for further processing in the EM system.

3. Results and discussion

3.1. 2-D EM analysis of VAT and VAT(ΔN)

The wild-type VAT monomer has a calculated molecular mass of 83 kDa, whereas the deletion mutant VAT(ΔN) has a calculated molecular mass of 63 kDa. This difference in mass is in accordance with the migration of the two proteins in SDS-PAGE analysis (Fig. 1b). Negatively stained (uranyl acetate) preparations of the two proteins have been examined by EM (Fig. 2). Both VAT and VAT(ΔN) form hexameric complexes imply that, in analogy to NSF, the N domain is not required for oligomerization [21]. The hexameric core of the wild-type and the mutant complex have similar shapes and dimensions. The diameter of the core structure is approximately 15 nm. Radial grooves which separate the six protomers from one another are outlined by staining and a prominent stain-filled center indicates the presence of a central channel. However, there are also distinct differences. The most conspicuous one is the presence of comma-shaped appendages in VAT at the periphery of the complex that emanate in a counter clockwise orientation from the corners of the hexagon. Their relatively low contrast is indicative of a rather flexible linkage to the core structure. Nevertheless, the difference map (VAT minus VAT(ΔN)) shown in Fig. 2a quite clearly depicts the location of this extra mass representing the N domain of VAT (residues 1–183). We conclude that the spatial arrangement of domains in VAT and probably other members of the subfamily 1 (see Section 1) is basically the same as described for NSF [21].

3.2. 3-D EM analysis of VAT and VAT(ΔN)

In order to obtain insights into the 3-D structure of VAT, we recorded electron tomographic tilt series of both the wild-type protein and the deletion mutant. Proteins were negatively stained with methylamine tungstate which preserves large protein structures remarkably well and minimizes flattening effects [36]. By automating data acquisition, we were able to keep the electron dose subcritical (see Section 2).

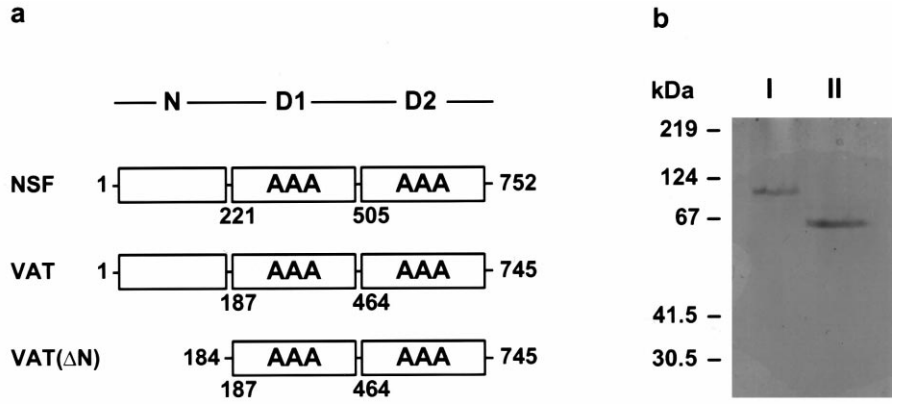

Fig. 1. (a) Domain maps of NSF, VAT and VAT(ΔN): D1 and D2 contain AAA-modules. The positions of D1 and D2 within the sequence of NSF and VAT (taken from [23] and [8]) are denoted by numbers underneath the boxes. (b) Coomassie blue-stained SDS-PAGE of VAT (I) and VAT(ΔN) (II) preparations.

At a first approximation, the averaged 3-D structure of VAT (Fig. 3a) can be described as a truncated cone with a height of 7 nm and diameters of 14–15 nm ('top') and 13–14 nm ('bottom'), respectively. A channel of 2–3 nm in diameter traverses the complex from end to end along the 6-fold axis. At the present resolution of 2.2 nm, the channel appears to be closed near the top. However, we do not know if this is a genuine feature of the structure or the result of local preparation-induced flattening. Such a channel appears to be a feature common to many AAA-ATPases. One could imagine that it has a role in unwinding of a polypeptide chain. After being pushed or pulled through the channel, the emerging chain has a new chance to refold, unless it is directed to a degradation machinery. In this sense, these AAA-ATPases may have an unfolding and folding function. The complex displays a distinct handedness throughout the core, indicating that the two domains which form the core (D1 and D2) are not in register but arranged with a stagger.

VAT(ΔN) has an overall structure similar to VAT (Fig. 3b) and does not differ as much as one might expect. The main difference between VAT and VAT(ΔN) is the presence of a feature accentuating the corners of the hexagon of VAT. This is located where the comma-shaped protrusions representing the N domain emanate in the difference map generated with uranyl acetate-stained samples (Fig. 2). The fact that only some rudimentary mass is observed at this location in the 3-D map of VAT indicates that the N domain is rather flexible in position in samples embedded in methylamine tungstate. In fact, in this stain, both VAT and VAT(ΔN) particles assume quite variable orientations with respect to the supporting film (as evidenced by the 3-D alignment parameters), while in uranyl acetate, the vast majority of particles are found in a unique orientation with the 'top' of the complex facing the carbon film. One could imagine that in this orientation, the N domain is stabilized in position and therefore appears more prominent in averages. On the other hand, 3-D reconstructions of VAT in uranyl acetate suffer from substantial flattening (data not shown).

Recently, the structure of the D2 domain of NSF has been solved to high-resolution by X-ray crystallography [23,24]. Since the D2 domain of NSF and VAT are quite similar (31% identity in the alignable regions: residues 500–634 of VAT, residues 545–681 from NSF, as judged by BLAST alignments using default parameters), it is expected that they have the same basic fold. Therefore, we took the crystal structure of NSF-D2 and, after low-pass filtering, fitted it into the bottom part of the VAT envelope as determined by electron tomography (Fig. 4). Obviously, the fit is quite satisfactory, since not only the outer boundary but also the central channel are almost congruent, thus lending support to the fidelity of the tomographic structure.

In NSF, the domains D1 and D2, which probably have the same fold, are believed to sit on top of each other [23,21]. Also in VAT, which has an overall height of 7 nm, there is room for two domains (D1 and D2) positioned on top of each other, particularly when arranged with a stagger. However,

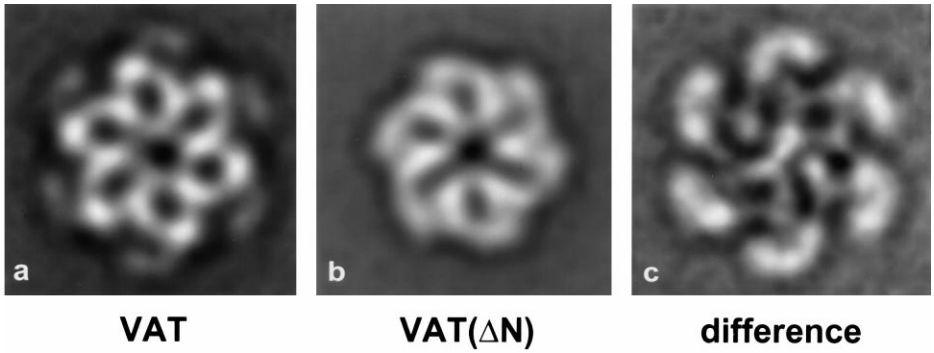

Fig. 2. Non-symmetrized 2-D averages of top views of (a) 388 VAT particles and (b) 499 VAT(ΔN) particles negatively stained with uranyl acetate. (c) Difference image generated by subtracting (b) from (a) after normalization.

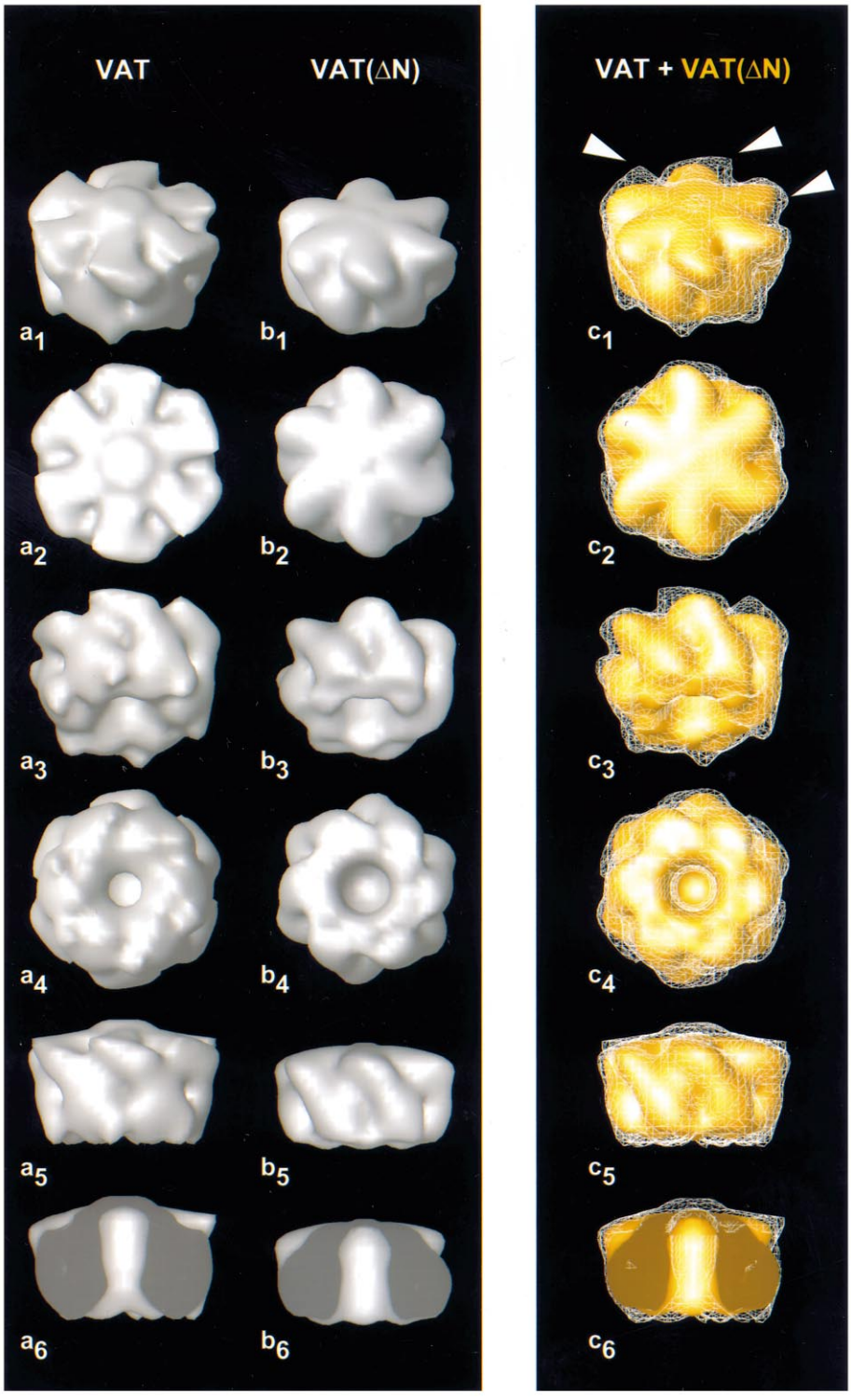

Fig. 3. Isosurface representations of the 3-D averages of VAT ($3a_1$–a_6) and VAT(ΔN) ($3b_1$–b_6) obtained by electron tomography after low-pass filtering to the resolution limit of 22 Å and a combined representation of VAT (white) and VAT(ΔN) (yellow) ($3c_1$–c_6). For all isosurfaces, threshold values were set to include the calculated molecular masses of VAT (500 kDa) and VAT(ΔN) (377 kDa) at an estimated protein density of 1.3 g/cm^3. 1: tilted top view, 2: top view, 3: tilted bottom view, 4: bottom view, 5: side view, 6: cut open view. Arrows mark the additional masses at the corners of the hexagon where, according to the map shown in Fig. 2, the N domains emanate. For details, see main text.

this arrangement leaves no room in the core region for the N domain. In fact, the projection data map this domain clearly to the periphery of the core where it appears to be flexibly linked to the D1 domain. Thus, it will be necessary to analyze large data sets of individual VAT particles in ice in order to describe the N domain more accurately and the conformational changes it might undergo during the catalytic cycle of this AAA-ATPase.

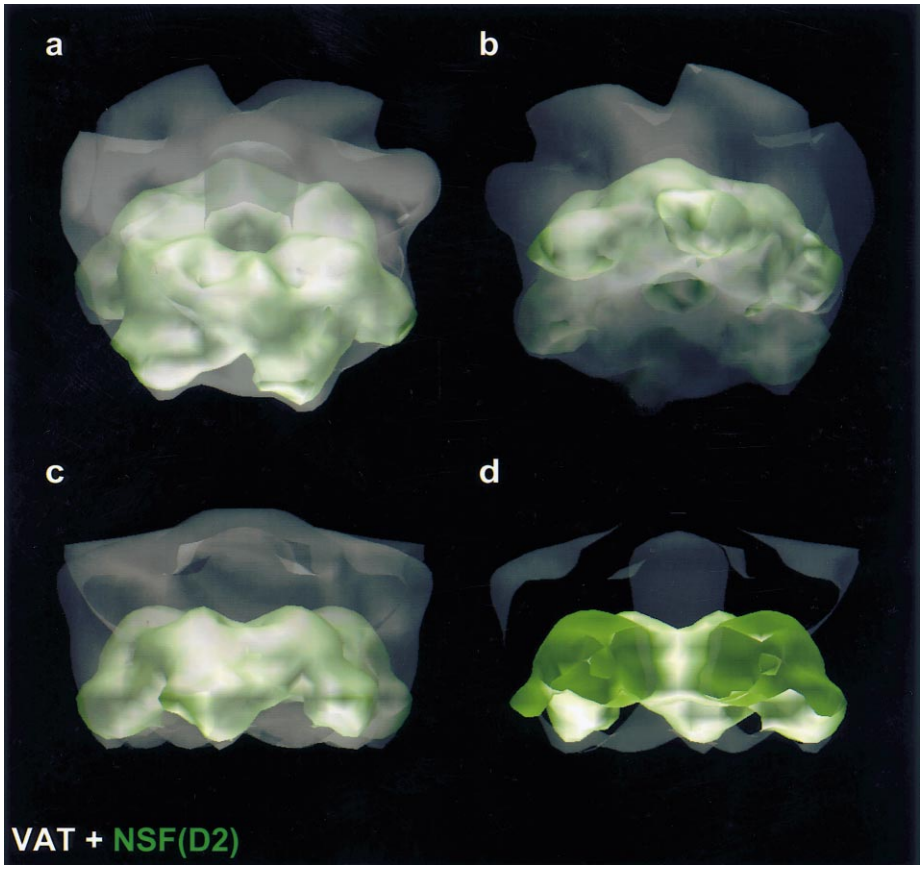

Fig. 4. An isosurface representation of the crystal structure of the D2 domain of NSF, low-pass-filtered to a resolution of 12 Å (green) combined with the 3-D structure of VAT (white) obtained by electron tomography, low-pass-filtered to a resolution of 22 Å. Threshold values were set to include the calculated molecular masses of VAT (500 kDa) and NSF(D2) (165 kDa). (a) tilted top view, (b) tilted bottom view, (c) side view, (d) cut open view.

Acknowledgements: We thank W.I. Weis for putting the NSF(D2) coordinates at our disposal before they were available in the Brookhaven Data Bank. This work was supported by postdoctoral fellowships from the Max-Planck-Gesellschaft and the Deutsche Forschungsgemeinschaft to B.R.

References

[1] Kunau, W.H., Beyer, A., Franken, T., Götte, K., Marzioch, M., Saidowsky, J., Skaletz-Rorowski, A. and Wiebel, F.F. (1993) Biochimie 75, 209–224.
[2] Walker, J.E., Saraste, M., Runswick, M.J. and Gay, N.J. (1982) EMBO J. 1, 945–951.
[3] Confalonieri, F. and Duguet, M. (1995) Bioessays 17, 639–650.
[4] Wolf, S., Nagy, I., Lupas, A., Pfeifer, G., Cejka, Z., Muller, S.A., Engel, A., DeMot, R. and Baumeister, W. (1998) J. Mol. Biol. 277, 13–25.
[5] Beyer, A. (1997) Protein Sci. 6, 2043–2058.
[6] Fröhlich, K.U., Fries, H.W., Rudiger, M., Erdmann, R., Botstein, D. and Mecke, D. (1991) J. Cell Biol. 114, 443–453.
[7] Peters, J.M., Walsh, M.J. and Franke, W.W. (1990) EMBO J. 9, 1757–1767.
[8] Pamnani, V., Tamura, T., Lupas, A., Peters, J., Cejka, Z., Ashraf, W. and Baumeister, W. (1997) FEBS Lett. 404, 263–268.
[9] Latterich, M., Fröhlich, K.U. and Schekman, R. (1995) Cell 82, 885–893.
[10] Rabouille, C., Levine, T.P., Peters, J.M. and Warren, G. (1995) Cell 82, 905–914.
[11] Beckers, C.J., Block, M.R., Glick, B.S., Rothman, J.E. and Balch, W.E. (1989) Nature 339, 397–398.
[12] Wilson, D.W., Wilcox, C.A., Flynn, G.C., Chen, E., Kuang, W.J., Henzel, W.J., Block, M.R., Ullrich, A. and Rothman, J.E. (1989) Nature 339, 355–359.
[13] Söllner, T., Bennett, M.K., Whiteheart, S.W., Scheller, R.H. and Rothman, J.E. (1993) Cell 75, 409–418.
[14] Wilson, D.W., Wilcox, C.A., Flynn, G.C., Chen, E., Kuang, W.J., Henzel, W.J., Block, M.R., Ullrich, A. and Rothman, J.E. (1989) Nature 339, 355–359.
[15] Tagaya, M., Wilson, D.W., Brunner, M., Arango, N. and Rothman, J.E. (1993) J. Biol. Chem. 268, 2662–2666.
[16] Whiteheart, S.W., Rossnagel, K., Buhrow, S.A., Brunner, M., Jaenicke, R. and Rothman, J.E. (1994) J. Cell Biol. 126, 945–954.
[17] Nagiec, E.E., Bernstein, A. and Whiteheart, S.W. (1995) J. Biol. Chem. 270, 29182–29188.
[18] Peters, J.-M., Harris, J.R., Lustig, A., Müller, S., Engel, A., Volker, S. and Franke, W.W. (1991) J. Mol. Biol. 223, 557–571.
[19] Fröhlich, K.U., Fries, H.W., Peters, J.M. and Mecke, D. (1995) Biochim. Biophys. Acta 1253, 25–32.
[20] Fleming, K.G., Hohl, T.M., Yu, R.C., Müller, S.A., Wolpensinger, B., Engel, A., Engelhardt, H., Brünger, A.T., Söllner, T.H. and Hanson, P.I. (1998) J. Biol. Chem. 273, 15675–15681.
[21] Hanson, P.I., Roth, R., Morisaki, H., Jahn, R. and Heuser, J.E. (1997) Cell 90, 523–535.
[22] Guenther, B., Onrust, R., Sali, A., O'Donnell, M. and Kuriyan, J. (1997) Cell 91, 335–345.
[23] Lenzen, C.U., Steinmann, D., Whiteheart, S.W. and Weis, W.I. (1998) Cell 94, 525–536.
[24] Yu, R.C., Hanson, P.I., Jahn, R. and Brünger, A.T. (1998) Nat. Struct. Biol. 5, 803–811.
[25] Schägger, H. and von Jagow, G. (1987) Anal. Biochem. 166, 368–379.

[26] Neuhoff, V., Arold, N., Taube, D. and Ehrhardt, W. (1988) Electrophoresis 9, 255–262.
[27] Dierksen, K., Typke, D., Hegerl, R., Koster, A.J. and Baumeister, W. (1992) Ultramicroscopy 40, 71–87.
[28] Hegerl, R. and Altbauer, A. (1982) Ultramicroscopy 9, 109–116.
[29] Hegerl, R. (1996) J. Struct. Biol. 116, 30–34.
[30] Van Heel, M. and Frank, J. (1981) Ultramicroscopy 6, 187–194.
[31] Harauz, G. and van Heel, M. (1986) Optik 73, 146–156.
[32] Radermacher, M., Wagenknecht, W., Verschoor, A. and Frank, J. (1986) J. Microsc. 141, 1–2.
[33] Walz, J., Typke, T., Nitsch, M., Koster, A.J., Hegerl, R. and Baumeister, W. (1997) J. Struct. Biol. 120, 387–395.
[34] Radermacher, M. (1988) J. Electron Microsc. Tech. 9, 359–394.
[35] Orlova, E.V., Dube, P., Harris, J.R., Beckman, E., Zemlin, F., Markl, J. and van Heel, M. (1997) J. Mol. Biol. 271, 417–437.
[36] Kolodziej, S.J., Penczek, P.A. and Stoops, J.K. (1997) J. Struct. Biol. 120, 158–167.